Structural differences between single crystal and polycrystalline UBe

Volz, Heather Michelle
Smith, Alice Iulia
Smith, James L.
Vogel, Sven C.
Fisk, Zachary
Dirmyer, Matthew R.
Judge, Elizabeth
Winkler, Bjorn

To be published in: Philosophical Magazine

DOI to publisher's version: 10.1080/14786435.2018.1468578

Permalink to record: http://permalink.lanl.gov/object/view?what=info:lanl-repo/lareport/LA-UR-17-21717

Structural Differences Between Single Crystal and Polycrystalline UBe_{13}

H.M. Volz[1], S.C. Vogel[1], A.I. Smith[1], J.L. Smith[1], Z. Fisk[2], B. Winkler[3], M.R. Dirmyer[1], E. Judge[1]

[1] *Los Alamos National Laboratory, PO Box 1663, Los Alamos, NM 87545*

[2] *Department of Physics & Astronomy, University of California, Irvine, CA 92697*

[3] *Fachbereich Geowissenschaften, Altenhöferallee 1, Goethe Universität, D-60438 Frankfurt, Germany*

Correspondence: Heather M. Volz, hvolz@lanl.gov, 1-505-665-4370

We report on observations of structural and chemical differences between samples of UBe_{13} that were synthesized using two different methods. Unexplained discrepancies in properties between samples with differing synthesis had previously been found in this heavy fermion superconductor. A polycrystalline UBe_{13} sample was made by arc-melting the constituents. Single crystals were grown using an aluminum flux and had a consistently slightly larger lattice parameter than the polycrystals, which merited further study. Neutron diffraction data were collected at the Lujan Center at LANSCE on the HIPPO diffractometer. Aluminum was detected by inductively coupled plasma mass spectrometry (ICP-MS) in the flux-grown single crystal (0.803 wt%), and small amounts (~0.2 wt%) of thorium were detected in the UBe_{13} polycrystalline sample. In order to probe the implications of the presence of Al, calculations by spin-polarized DFT-GGA+U show that the incorporation of Al onto the *96i* site (the lowest symmetry site in the structure) is energetically more favorable than on other sites. In general, the trends calculated by DFT for bond lengths and lattice parameter increases are consistent with bond lengths experimentally observed by neutron diffraction, but specific percentage changes with aluminum incorporation may be obscured by the unexpected thorium in the polycrystalline sample. The aggregate of our initial observations suggests that incorporation of aluminum from the flux into single crystal UBe_{13} is significant.

Keywords: heavy-fermion, synthesis, impurities, crystal, neutron diffraction

Introduction

The compound UBe_{13} is the only intermetallic phase in the uranium-beryllium system that is known to be stable at temperatures below the melting point of pure uranium. See phase diagram in Figure 1 [1]. UBe_{13} has been a scientifically intriguing material due to its atypical behavior. Historically, it was realized that if the interatomic spacing of uranium atoms is small in a uranium compound, the atoms have a tendency to form bands and can be superconducting. If uranium atom spacing were larger, the atoms usually possess magnetic moments and could order magnetically, as antiferromagnets or ferromagnets. This is shown in the Hill Plot in Figure 2 [2, 3, 34], and this observation was largely independent of intervening atoms on a lattice, unless the other atoms exhibited similar spacing effects such as Ce or Pu.

Then in 1983, the superconductivity of UBe_{13} was discovered [4] with very widely spaced U atoms. However, the specific heat was anomalously large, possessing more similarities to magnets. In time, work with actinide and cerium compounds led to a class of heavy fermion superconductors, which show very high electrical resistivities from intense electron scattering that is still not fully understood and in most cases a tendency to become magnetic with small perturbations. With small amounts of substitutional thorium, *i.e.,* as $U_{1-x}Th_xBe_{13}$, this compound still exhibits superconductivity, albeit altered with another transition in the specific heat [5-8].

Small amounts of impurities within a crystallographic lattice are known to have a remarkable impact on observed behavior. As work by Smith has shown [9], the behavior of impurities in UBe_{13} has drastic implications for resistivity, superconducting transition temperature, and electron pairing in this compound. At that time, it was suspected that aluminum impurities were present in the single crystals, as they were precipitated from an aluminum solvent. Single crystals of UBe_{13} have slightly different physical properties than polycrystalline samples, including lower T_c, broader transition regions, and less-sharp resistivities, as well as a slightly but significantly larger lattice parameter. Attempts to confirm the observed trend by re-creating the observations in arc-melted polycrystalline samples with aluminum intentionally added as an impurity were unsuccessful. Note that other impurities in UBe_{13} (for example, B, Cu, and Ga on Be sites) destroy the superconductivity; off-stoichiometry UBe_{13} samples have lattice parameters almost identical to the stoichiometric polycrystalline material [9]. The goal of the study presented here was to show whether aluminum on one of the Be sites in the single crystals accounted for the larger lattice parameter in the single crystals.

Although sample fabrication and initial work on crystallographic characterization were complete years ago, a large volume of research on UBe_{13} is still being conducted, as this heavy fermion system is still relevant today to understand *f*-electron physics and unconventional superconductivity. Theories and models to explain UBe_{13} anomalous properties (with new experimental data) continue to be discussed. See, for example, [10-13]. Our intent with this work is to examine the degree to which impurities are present in these older samples, despite the seemingly pure phases when measured years ago by diffraction [9]. With chemical knowledge and with information on atomic positions of impurities, more accurate theoretical modeling can be performed.

The crystallographic structure (measured on single crystals) is given in [14] as *Fm3c* with a=10.268(2). It is the $NaZn_{13}$-type structure, with U atoms on the *8a* Wycoff positions at (¼, ¼, ¼); Be-1 on the *8b* positions at (0,0,0); and Be-2 on the *96i* positions (0,y,z) with y=0.115 and z=0.177. See Figure 3.

In this work, samples of polycrystalline and single crystal UBe_{13} samples were analyzed using neutron diffraction to look for slight differences and to attempt to determine crystallographic reasons for the observed changes in physical properties without the loss of superconductivity. DFT calculations were also performed and compared to experimentally observed crystallographic properties. Finally, chemical analysis methods were used to check the purity of the samples made by the two methods.

Experimental

Polycrystalline UBe_{13} samples were made by arc-melting, repetitively turning and re-melting the constituents (at least 6 repeats) on a copper water-cooled hearth in an argon atmosphere. [16]

Single crystals were made by dissolving the constituents in aluminum at 1200°C in a beryllia crucible and slow cooling. Then aluminum is leached out with concentrated NaOH to reveal the crystals. Single crystals solidify at a much lower temperature (approximately 1000°C lower) and were cooled at a much slower rate than the polycrystals.

For this work, both polycrystalline and single crystal sample types were pulverized and sieved through 38 μm screens, then sealed into vanadium cylindrical test canisters.

Neutron scattering measurements were made at the Lujan Center at LANSCE (Los Alamos, NM) on the high-pressure preferred orientation (HIPPO) diffractometer [17, 18] in October, 2009. Data from a control can was collected as part of the routine operation of the flight path (FP4). Neutron diffraction measurements were collected at room temperature and ambient pressure on the HIPPO instrument. Data were subsequently analyzed by Rietveld refinement, using the General Structure Analysis System (GSAS) [19]. Data on the single crystal and polycrystalline samples were collected on the HIPPO instrument for count times corresponding to 104 and 106 minutes at 100 micro-Ampere proton current, respectively.

An attempt was made to detect aluminum contents in the two different samples by neutron activation, but the short half-life of ^{28}Al of only 2.2414 minutes was too short to overcome the logistics between irradiation in the thermal or fast neutron beams and spectrometer. The results of this approach were therefore inconclusive.

Chemical analysis by inductively coupled plasma mass spectrometry (ICP-MS) was performed. Approximately 45 mg of each sample was digested at room temperature in 5 grams of high purity Optima grade nitric acid. Deionized water (18.3 MΩ) was added to the sample to bring the total mass up to 20 grams. This solution was further diluted to an appropriate concentration. The samples were analyzed with two dilutions, 1:50 and 1:500, using 2% HNO_3 as the diluent. Elemental standards were prepared at 5, 15, 25, 35, and 45 ppb concentrations for Al. All ICP-MS samples and standards were spiked with an indium internal standard (10 ppb). Each dilution was analyzed with a separate set matrix matched standards with respect to U and Be concentrations. An acid blank was also prepared as each sample and was found to have no aluminum; therefore no blank correction was applied. Standard deviations were calculated based on triplicate instrument analysis.

Spin-polarized density functional theory (DFT) calculations were performed with commercial and academic versions of the CASTEP program [20] using a generalized gradient approximation PBE-GGA [21] on the 'on the fly' pseudopotentials from the CASTEP 8.0 data base and a Hubbard U of 2 eV for the f-electrons of uranium. The maximum cut-off energy of the plane waves was 480 eV. Monkhorst–Pack grids [22] were employed for sampling of reciprocal space, corresponding to a k-point separation of less than 0.030 $Å^{-1}$. Elastic stiffness coefficients were obtained from stress-strain relations [23]. Full geometry optimisations were carried out until forces were smaller than 0.01 eV A^{-1} and no component of the stress tensor exceeded 0.02 GPa. The accuracy of the approach was established by computing structures and properties for Al, Be and UBe_{13} and comparing these to available experimental data.

Results

Chemistry

Chemical analysis of the UBe_{13} solutions was carried out on a Thermo Scientific iCAP Q ICP-MS. Calibration curves were obtained with a correlation coefficient of greater than 0.995 for Al. The 1:500 dilution was used to calculate the Al weight percent for sample ID 1986 (the crushed single crystal); whereas the 1:50 dilution was used to calculate the Al weight percent for sample ID 3318 (the polycrystalline sample). Furthermore, the polycrystalline sample was observed to have a concentration of thorium on the order of 0.2 wt% as determined by the survey scan.

The results of the analysis are presented in Table 1 and represent the concentrations of aluminum in these samples. Note that 0.8 wt% Al is ~$U(Be_{12.9}Al_{0.1})$

Density functional theory (DFT)

DFT was used to examine the energetics of possible aluminum atoms substitutionally on the three different atomic positions. To establish the reliability of the calculations and used parameters, Table 2, Table 3, and Table 4 provide a comparison for experimental and computed parameters for pure aluminum, pure beryllium, and UBe_{13}, respectively.

To summarize the calculations, the current work predicts the physical properties of the relevant phases within the typical limits of DFT-GGA+U calculations. Specifically, the elastic stiffness coefficients of beryllium are reproduced within 10% of the experimental values. The elastic properties of UBe_{13} should not differ substantially from those of beryllium. The negative value for the low temperature elastic stiffness coefficient C12 given in [30] is unphysical and our calculations yield a positive value for this tensor component. Based on the reasonable agreement between the structures and properties of UBe_{13}, Al, and Be, we use the total energies to extract relative stabilities.

Using calculations mostly based on a 2x1x1 supercell, *e.g.* $U_{32}Be_{416}$, we find that Al substitutes preferentially on Wyckoff position *96i*, as the incorporation of Al on this site is substantially (~ 125 kJ/mol) more favorable than incorporation on the *8b* site. We did not test for incorporations in interstitial sites.

More information on the DFT results in regards to bond lengths and lattice parameter changes are given in the following section when considering the experimentally determined values by Rietveld refinement, as well as in the Discussion section.

The results of our calculations imply that, in fact, a few atomic percent of aluminum can be incorporated into UBe_{13}, which is explored experimentally by ICP-MS and neutron diffraction for these two samples. However, an accurate determination of the amount of Al that can be incorporated would require a detailed treatment of the effects of long- and short-range ordering and therefore was beyond the scope of this study.

Neutron scattering

Both the ground single crystal and ground polycrystalline samples exhibited high quality neutron diffraction patterns, with low background. Simultaneous Rietveld refinement with the GSAS software against diffraction patterns of the 144 degree, 90 degree, and 40 degree full ring detectors was conducted using the gsas_language [32] with the following refinement strategy: In the first step, 8 background parameters of the GSAS background function #1 and the histogram scale for each histogram were fit. To adjust for slight sample misalignment, the time-of-flight (TOF) to d-spacing conversion parameters, 'DIFC,' were refined for the 90 and 40 degree histograms while the DIFC for the 144 degree histogram was kept constant at the calibration value. The lattice parameter was also refined in this second step. The isotropic thermal motion parameters of all three atoms and followed by atomic positions *y* and *z* of the *96i* Be atom and diffraction peak width parameter ‘sigma_1’ were refined in the next steps. To adjust for absorption or overestimation of the incident intensity, TOF absorption parameters were refined afterwards. The *96i* Be atom allows for anisotropic thermal motion parameters, which refined in the next step. Since chemical analysis indicated the presence of Th (presumed to be on the U position) and the presence of Al (presumed to be on the Be positions), with the DFT calculations indicating a clear preference for Al on the *96i* Be position, we copied the U and 96 Be atoms and changed the atom types to Th and Al, respectively. The thermal motion parameters and atomic positions were appropriately constrained to be identical while the site occupation factors were constrained to add to unity. To account for the fact that the materials were synthesized with depleted uranium, the U atom was replaced with the 238U isotope. The neutron scattering lengths for 238U and Th are 8.402 fm and 10.31 fm, respectively, while those for Be and Al are 7.79 fm and 3.449 fm, respectively [33]. The largest number of refined parameters for the 9493 data points was 45 and all refinement steps converged, *i.e.,* no parameter oscillations were observed.

Table 5 gives final refined values for the two different samples, using the starting structure by McElfresh [14] for refinement.

The reduced chi-squared for the refinement of U/Th site occupation reduced from 16.71 after anisotropic thermal motion refinement to 16.30 in the case of the single crystal and from 10.82 to 10.38 in the case of the polycrystalline sample. However, in both cases the uranium site occupation factor resulted in unphysical values of 1.20(2) and 1.24(2). The refinement of the site occupation for U/Th was therefore left out. For the Be/Al on the *96i* site, we found that the reduced chi-squared dropped from 16.64 after the refinement of anisotropic thermal motion parameters to 16.49 for the single crystal sample and from 10.76 to 10.55 for the polycrystalline sample. The refined site occupation factors for Be were 1.018(4) and 1.038(4) for the single crystal and polycrystalline samples, respectively. Attempts to refine Al site occupation on the Be1 *8b* site resulted in similarly unphysical Be occupancies. We therefore conclude that the neutron diffraction analysis is not sensitive to the refinement of Al and Th contamination and conducted the final refinement without those variables. All values reported in Table 5 therefore correspond to refinement with pure U and Be.

The final reduced chi-squared (χ^2) values for the refinements of the single crystal and polycrystalline datasets without refinement of site occupation factors were 16.52 and 10.64, respectively, and the final refinement for the 90 degree detectors for both samples are shown in Figure 4 and Figure 5. The refinement results are compiled in Table 5 with the uncertainties reported by GSAS in parentheses.

Discussion

Consistent with earlier work, we observe that the ground single crystal powder results in a significantly larger lattice parameter and unit cell volume than the ground arc-melted polycrystalline samples. In our case the increase in lattice parameter is 0.0045 Å or 0.04%. The other crystallographic parameters do not show as significant of differences between the refined parameters for the two samples. These numbers from neutron diffraction data are slightly smaller overall than X-ray diffraction numbers, which were 10.2656 and 10.255 Å, for single and polycrystal, respectively (a change of 0.1%) [9].

In the DFT calculations discussed in the earlier Results section, the incorporation of Al leads to a small increases in the cell volume, where an incorporation of 1% leads to an increase of the lattice parameter of about 1.4%. As shown in the neutron diffraction results, a small change in lattice parameter occurred but was smaller (0.04%) than the predicted 1.4%. However, the presence of thorium in the polycrystalline UBe_{13} was not expected and implications are not understood at this time. Supercell calculations such as those performed here by DFT are not well suited to study the incorporation of small amounts of defects, as unit cells need to be very large in order to avoid a spurious self-interaction of the defect with a symmetry-related defect site nearby.

Despite these challenges in obtaining precise impurity atom locations by DFT calculation and diffraction experiment, we must emphasize our primary point in this paper is the experimental observation of the existence of impurities in the UBe_{13} (despite the continued presence of superconductivity in this heavy fermion superconductor, published elsewhere [9]) that could have important ramifications on modelling work. Moreover, chemically detected aluminium is indeed shown to be energetically favorable on the *96i* site whereas prior work in the literature does not appear to have considered impurities in UBe_{13} models. From these first results in this heavy fermion superconductor structural study, the significantly expanded unit cell (by 45 σ, see Table 5) is the most noteworthy difference among the data from two impure samples with different preparation methods.

In addition to the lattice parameter changes, results from the DFT calculations gave bond lengths for pure UBe_{13} that were comparable to those experimentally observed in the neutron diffraction data (Table 5). For the incorporation of aluminum on the *8b* (0,0,0) site, from DFT calculations the Al-Be bond length would be approximately 2.22 Angstroms; on the *96i* site, there would be a range of Al-Be bonds in lengths 2.26-2.45 Angstroms. Both of these bond lengths resulting from Al incorporation are larger than those for comparable Be-Be bonds in pure

UBe_{13}. Although the observed bond lengths from both samples in Table 5 are very close to each other (and within experimental error for Be2-Be2 atoms on Wyckoff *96i* sites), it is interesting that the overall trends for the single crystal sample containing aluminum had larger bond lengths and larger lattice parameter than the polycrystalline sample, which was indeed the trend calculated by DFT. These trends and comparison between results by DFT calculations and experimentally obtained neutron diffraction data adds to the evidence that Al sits on the *96i* site.

The difference Fourier maps generated by GSAS for the cases with fixed site occupation factors are visualized with VESTA [15] in Figure 6a and Figure 6b. The difference map densities range from F_min=-0.357 to F_max=0.194 and F_min=-0.366 to F_max=0.185 for the single crystal and polycrystalline samples, respectively. As can be seen in Figure 6a and Figure 6b, where Fourier difference maps are plotted for both cases with difference densities above 0.15 in magnitude of either positive or negative density, the negative maxima are located at the U positions, indicating that the diffraction data suggest less scattering density at the uranium location. This decrease is consistent with the site occupation factor moving towards the lower scattering length element when refining U and Th occupation described above. Refinement of the site occupation factors of U atoms without balancing with a second element, *i.e.* refining vacancy concentration on the U site, lead to uranium site occupation factors of 0.965(3) and 0.949(3) and reduced chi-squared of 16.32 and 10.38 for refinements from single crystal and polycrystalline samples, respectively. However, the magnitude of the negative difference Fourier map minima changed only slightly (e.g. from F_min=0.357 to F_min=0.344 for the single crystal) and the visualization had essentially the same appearance as before, *i.e.* the refinement was not improved dramatically. The energetically favorable position for thorium was not conclusive in this work, but we suggest that researchers studying arc-melted polycrystalline UBe_{13} should confirm their sample purity with respect to Th. Based on our initial analysis of this material, we suspect Th is substitutional on the U site.

Conceptually, upon study of Table 5 and Figure 3, we infer that the incorporation of Al results in Be icosahedra that remain roughly constant, but that the U-Be2 atomic distance slightly expands to result in the larger lattice parameter. In other words, the lattice parameter is enlarged by expansion in distances between icosahedra, rather than changes to the icosahedra themselves. Future work could examine whether superconductivity may be impacted differently if an impurity element incorporates into the structure in a different manner, but we are cautious and emphasize that this is an initial examination of the impurities in the structure and further work is needed.

Conclusions

As in prior work, analysis of the diffraction patterns from two samples of UBe_{13} prepared by different methods resulted in significant differences in unit cell parameters. From ICP-MS chemical analysis, Al-flux grown single crystal samples of UBe_{13} contained aluminum at 0.803 wt%, presumed to be incorporated from the flux during the growth process. Although arc-melted polycrystalline samples contained much less aluminum (by over an order of magnitude), they were found to contain thorium. Both samples were ground and sieved prior to analysis.

DFT calculations show that the aluminum is energetically most favorable on the low symmetry *96i* site, and can accommodate a few at%. The experimental bond lengths and lattice parameters (from diffraction data) showed increases when comparing polycrystalline to single crystal UBe_{13} but the largest changes were in lattice parameter. The results indicate the Be icosahedra may be remaining fairly constant in size, but expanding out from the U atoms when

Al is present. A better understanding of occupancies and atomic positions in this system, as well as more complete validation between experiment and calculation, would need more modeling on the possible locations of Th atoms in the polycrystalline sample for comparison, or a range of samples with varying impurity concentrations for experimental diffraction measurements. Although beyond the scope of this work, it would be useful to further modela range of possible effects of aluminum on lattice defects in UBe_{13}, with an eye towards matching the experimentally observed change in lattice parameter with Al present.

The reasons for continued superconductivity in UBe_{13} single crystals with aluminum present, when other elements destroyed the behavior, are hitherto unknown. Yet, our experimental and DFT results show that not only is aluminium chemically present but also energetically favorable on the low symmetry site. Although we still have unanswered questions, these first results are being presented to the community for consideration. More work in the future could determine atom positions more precisely. The implications of these impurities (and comparisons among different impurity elements) within a heavy fermion superconductor would be an interesting future area of study.

Acknowledgements

This information has been authored by an employee or employees of the Los Alamos National Security, LLC. (LANS), operator of the Los Alamos National Laboratory under Contract No. DE-AC52-06NA25396 with the U.S. Department of Energy.

References

[1] R.W. Buzzard, "Beryllium-Uranium System," *J. of Research of the National Bureau of Standards,* Vol. 50 Number 2, (1953) pp. 63-67.

[2] H.H. Hill, *Plutonium 1970 and Other Actinides*, W.N. Miner, ed., American Institute of Mechanical Engineers, New York, NY, 1970.

[3] Z. Fisk, H.R. Ott, and J.L. Smith, *Chemical Physics of the heavy electron uranium compounds,* J. Less-Common Metals 133 (1986), pp. 99-106.

[4] H.R. Ott, H. Rudigier, Z. Fisk, and J.L. Smith, *UBe_{13}: An unconventional actinide superconductor,* Phys. Rev. Lett. 50 (1983), p.1595-1598.

[5] H.R. Ott, H. Rudigier, E. Felder, Z. Fisk, and J.L. Smith, *Influence of impurities and magnetic fields on the normal and superconducting states of UBe_{13}*, Phys. Rev. B 33 (1986), p. 126-131.

[6] M.B. Maple, *Interplay between superconductivity and magnetism,* Physica B 215 (1995), pp. 110-126.

[7] C. Pfleiderer, *Superconducting phases of f-electron compounds,* Rev. Mod. Phys. 81 (2009), pp. 1551-1624.

[8] Z. Fisk, H.R. Ott, T.M. Rice, and J.L. Smith, *Heavy-electron metals,* Nature 320 (1986), pp.124-129.

[9] J.L. Smith, Z. Fisk, J.O. Willis, H.R. Ott, H. Rudigier, *Impurity effects in UBe_{13},* Physica 135B (1985), pp. 3-8.

[10] Y. Shimizu, Y. Haga, Y. Ikeda, T. Yanagisawa, and H. Amitsuka, *Observation of an unusual magnetic anomaly in the superconducting mixed state of heavy-fermion compound UBe_{13} by precise dc magnetization measurements,* Phys. Rev. Lett. 109 (2012), p. 217001.

[11] Y. Shimizu, S. Kittaka, T. Sakakibara, Y. Haga, E. Yamamoto, H. Amitsuka, Y. Tsutsumi, and K. Machida, *Field-orientation dependence of low-energy quasiparticle excitations in the heavy-electron superconductor UBe_{13}*, Phys. Rev. Lett. 114 (2015), pp. 147002.

[12] V.G. Storchak, J.H. Brewer, D.G. Eschchenko, P.W. Mengyan, O.E. Parfenov, A.M. Tokmachev, P. Dosanjh, Z. Fisk, and J.L. Smith, *Spin gap in heavy fermion compound UBe_{13},* New J. Physics 18 (2016), p. 083029.

[13] A. Hiess, A. Schneidewind, O. Stockert, and Z. Fisk, *Signature of superconductivity in UBe_{13} as seen by neutron scattering: Superconducting and magnetic energy scales,* Phys. Rev. B 89 (2014), p. 235118.

[14] M.W. McElfresh, J.H. Hall, R.R. Ryan, J.L. Smith, *Structure of the heavy-fermion superconductor UBe_{13},* Acta Cryst. C46 (1990), pp. 1579-1580.

[15] K. Momma and F. Izumi, *VESTA 3 for three-dimensional visualization of crystal, volumetric and morphology data,* J. Appl. Cryst. 44, (2011), pp. 1272-1276.

[16] J.L. Smith, Z. Fisk, J.O. Willis, B. Batlogg, and H.R. Ott, *Impurities in the heavy-fermion superconductor* UBe_{13}, J. Appl. Phys., 55 (1984), pp. 1996-2000.

[17] H.R. Wenk, L. Lutteroti, S.C. Vogel, *Texture analysis with the new HIPPO TOF diffractometer,* Nucl. Instr. Methods Phys. Res. A 515 (2003), pp. 575-588.

[18] S.C. Vogel, C. Hartig, L. Lutterotti, R.B. Von Dreele, H.R. Wenk, and D.J. Williams, *Texture measurements using the new neutron diffractometer HIPPO and their analysis using the Rietveld method,* Powder Diffraction 19 (2004), pp. 65-68.

[19] A.C. Larson and R.B. Von Dreele, *General Structure Analysis System (GSAS),* Report LAUR-86-748, Los Alamos National Laboratory, 1994.

[20] S.J. Clark, M.D. Segall, C.J. Pickard, P.J. Hasnip, M.I.J. Probert, K. Refson, M.C. Payne, *First principles methods using CASTEP*, Zeitschrift für Kristallographie-Crystalline Materials 220 (2005), pp. 567–570.

[21] J.P. Perdew, K. Burke, M. Ernzerhof, *Generalized gradient approximation made simple,* Phys. Rev. Lett. 77 (1996), pp. 3865–3868.

[22] H.J. Monkhorst and J.D. Pack, *Special points for Brillouin-zone integrations,* Phys. Rev. B 13 (1976), pp. 5188-5192.

[23] V. Milman and M.C. Warren, *Elasticity of hexagonal BeO,* J. Phys.: Condensed Matter 13 (2001), pp. 241-251.

[24] W. Witt, *Absolute praezisionsbestimmung von gitterkonstanten an germanium- und aluminium-einkristallen mit elektroneninterferenzen*, Z. Naturforsch. 22A (1967), pp. 92-95.

[25] A.M. James and M.P. Lord, *Macmillan's Chemical and Physical Data*, Macmillan, London, UK, 1992.

[26] G.W.C. Kaye and T.H. Laby, *Tables of Physical and Chemical Constants*, Longman, London, UK, 15th ed., 1993.

[27] G.V. Samsonov (ed.), *Handbook of the Physicochemical Properties of the Elements*, IFI-Plenum, New York, USA, 1968.

[28] A. Migliori, H. Ledbetter, D.J. Thoma, T.W. Darling, *Beryllium's monocrystal and polycrystal elastic constants,* J. Appl. Phys. 95 (2004), pp. 2436-2440.

[29] K.J.H. Mackay and N.A. Hill, *Lattice parameter and hardness measurements on high purity beryllium*, J. Nucl. Mater. 8 (1963), pp. 263-264.

[30] R.A Robinson, J.D. Axe, A.I. Goldman, Z. Fisk, J.L. Smith, H.R. Ott, *Measurement of acoustic phonons in* UBe_{13}, Phys. Rev. B 33 (1986), pp. 6488-6490.

[31] U. Benedict, S. Dabos, L. Gerward, J. Staun Olsen, J. Beuers, J.C. Spirlet, and C. Dufour, *Study of the heavy-fermion compounds under high pressure,* J. Magn. Magn. Mater. 63-64 (1987), pp.403-405.

[32] S.C. Vogel, *gsaslanguage: A GSAS script language for automated Rietveld refinements of diffraction data,* J. Appl. Cryst. 44 (2011), pp. 873-877.

[33] *Neutron scattering lengths and cross-sections* in Neutron News, Vol. 3, No. 3, (1992), pp. 29-37. Available at https://ncnr.nist.gov/resources/n-lengths/

[34] H.R. Ott and Z. Fisk, *Heavy-Electron Actinide Materials*, in *Handbook of the Physics and Chemistry of the Actinides*, A.J. Freeman and G.H. Landereds, eds., Elsevier, Amsterdam, 1987, p. 85.

Figure Captions:

Figure 1: U-Be binary phase diagram [1].

Figure 2: Critical temperature T_C for superconductivity and Neel temperature T_N for magnetic order for uranium compounds as a function of U-U spacing [34]

Figure 3: Crystal structure of UBe_{13} with Be1 on position (0,0,0) coordinated by 12 Be2 atoms forming icosahedra. Uranium atoms (grey in color) are located on (1/4, 1/4, 1/4) positions. Be atoms in green. Shown using Visualization for Electronic and STructural Analysis (VESTA), [15].

Figure 4: Rietveld refinement of neutron diffraction pattern from ground single crystal UBe_{13}

Figure 5: Rietveld refinement of neutron diffraction pattern from ground polycrystalline UBe_{13}

Figure 6: Difference Fourier maps visualized by VESTA [15]. (a) is from the ground single crystal UBe_{13} and (b) is from the ground polycrystalline sample.

Table titles:

Table 1: Concentration of aluminum in the two samples prepared by different means, corrected for dilution factor

Table 2: Aluminum [24, 25, 26, 27]

Table 3: Beryllium [28, 29]

Table 4: UBe_{13} [9, 14, 30, 31]

Table 5: Neutron diffraction results from Rietveld refinement. Error in last digit in parenthesis

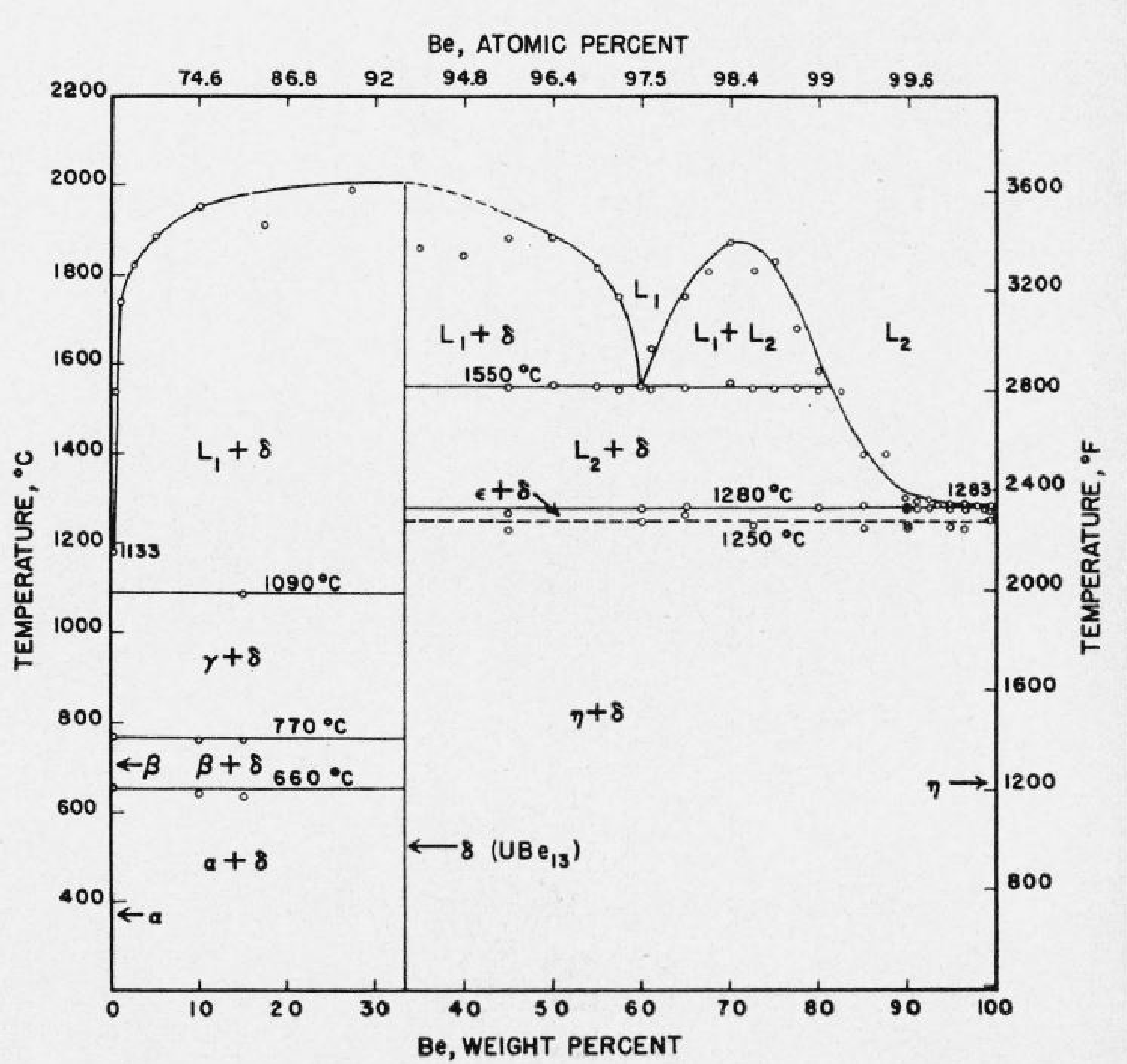

Be, ATOMIC PERCENT
74.6
86.8
92
94.8
96.4
97.5
98.4
99
99.6
TEMPERATURE, °C
TEMPERATURE, °F
L1
L1 + δ
L1 + L2
L2
1550 °C
L2 + δ
ε + δ
1280 °C
1283
1250 °C
1133
1090 °C
γ + δ
770 °C
←β
β + δ
660 °C
α + δ
←α
η + δ
η →
← δ (UBe13)
Be, WEIGHT PERCENT

Figure 2: Critical temperature T_C for superconductivity and Neel temperature T_N for magnetic order for uranium compounds as a function of U-U spacing [2, updated in 3]

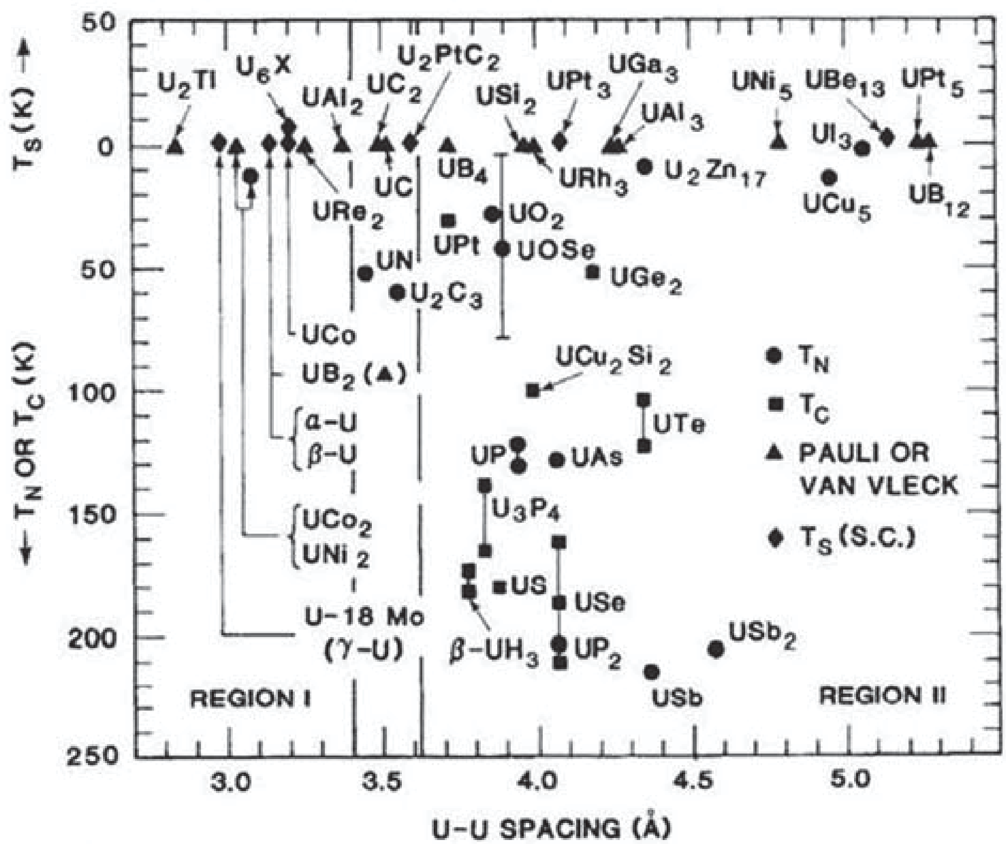

Figure 3: Crystal structure of UBe_{13} with Be1 on position (0,0,0) coordinated by 12 Be2 atoms forming icosahedra. Uranium atoms (grey in color) are located on (1/4, 1/4, 1/4) positions. Be atoms in green. Shown using Visualization for Electronic and STructural Analysis (VESTA), [15].

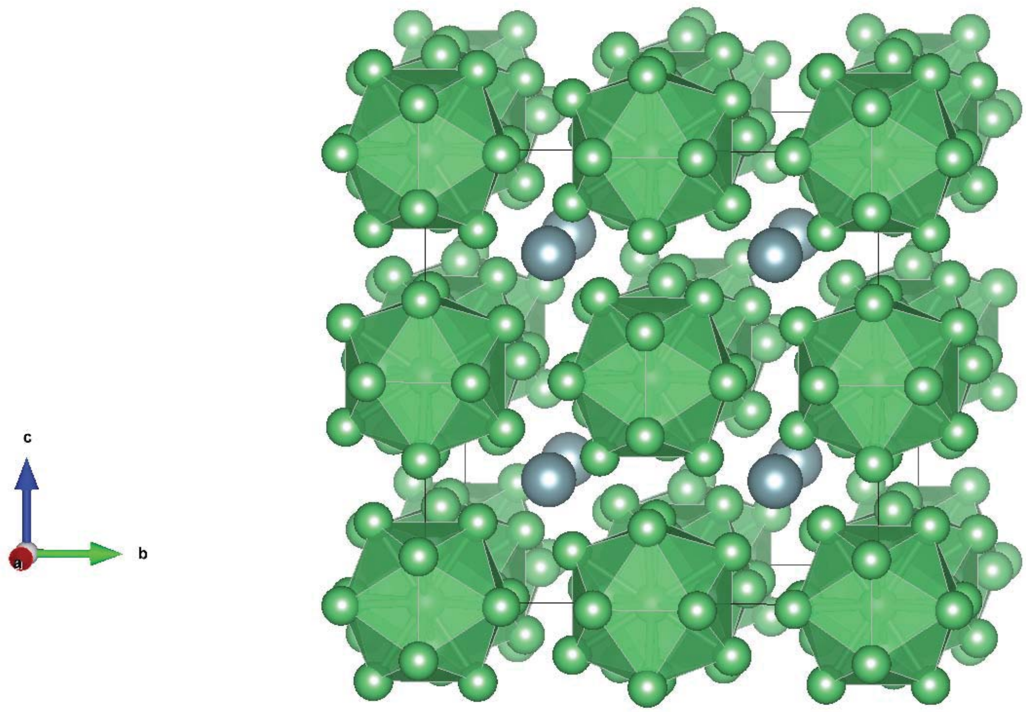

Figure 4: Rietveld refinement of neutron diffraction pattern from ground single crystal UBe_{13}

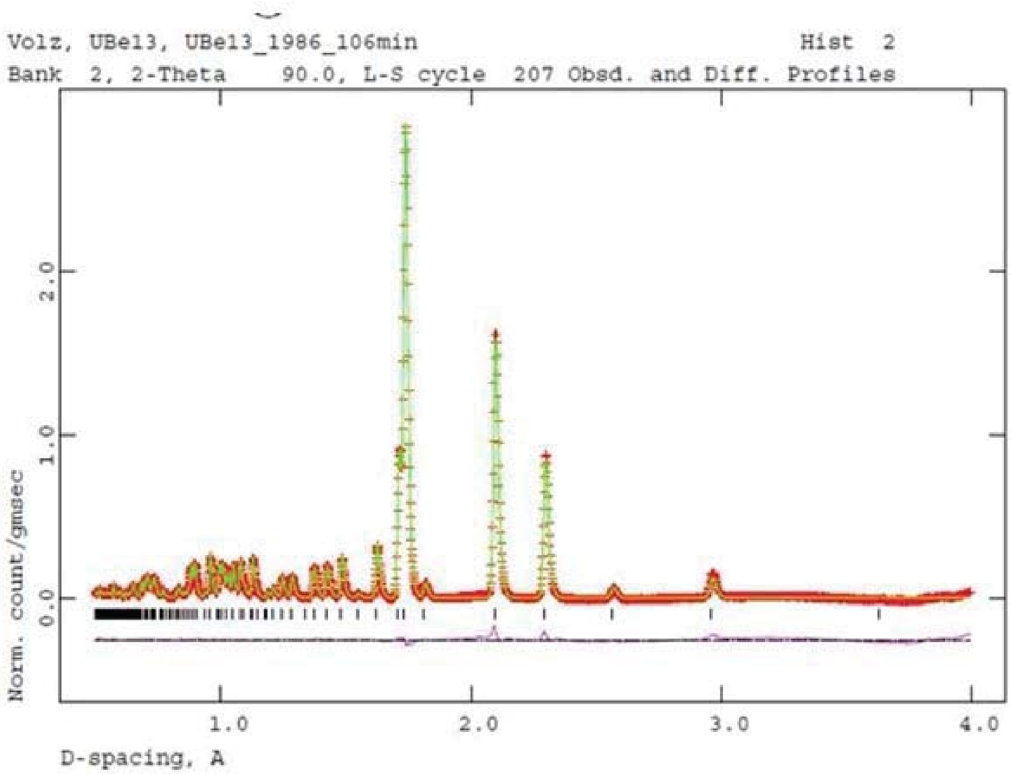

Figure 5: Rietveld refinement of neutron diffraction pattern from ground polycrystalline UBe_{13}

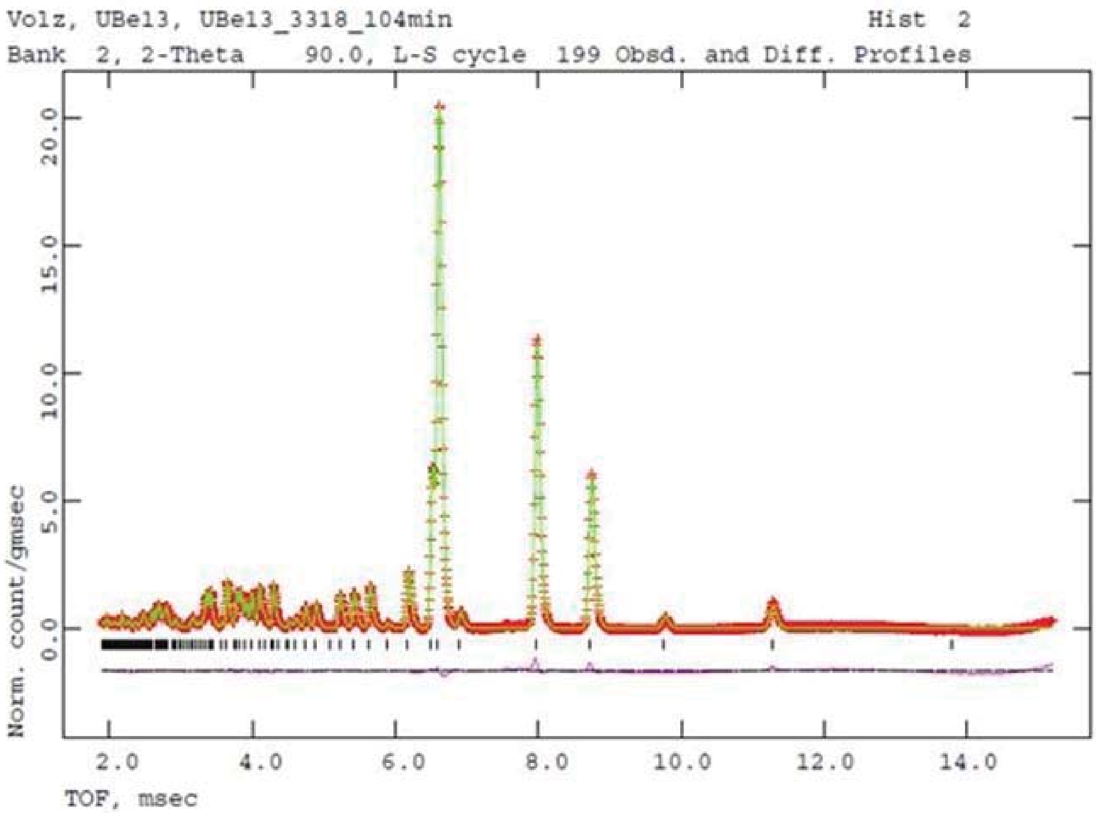

Figure 6: Difference Fourier maps visualized by VESTA [15]. (a) is from the ground single crystal UBe_{13} and (b) is from the ground polycrystalline sample.

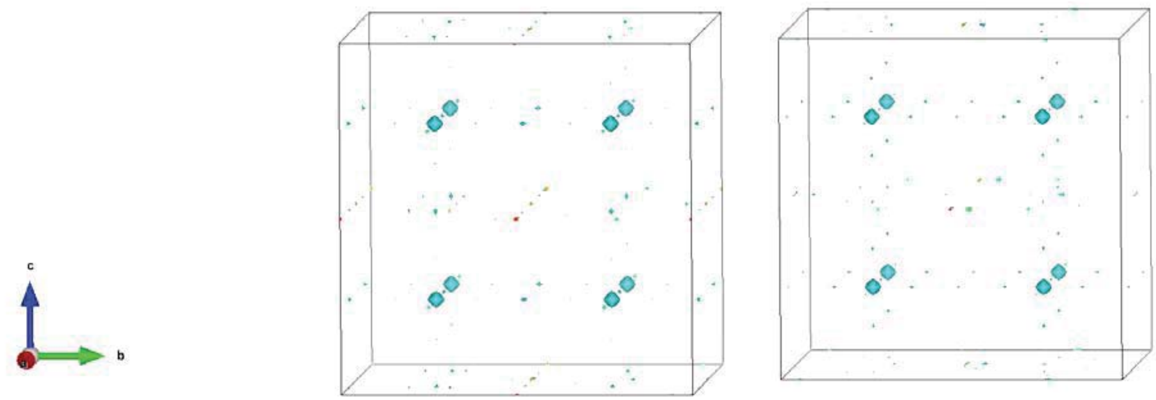

Table 1: Concentration of aluminum in the two samples prepared by different means, corrected for dilution factor

Sample	Aluminum in wt% (27 Al)	Sigma
Single crystal, ground and sieved (38 micron)	0.803	2.52x10-2
Polycrystalline specimen, ground and sieved (38 micron)	0.0198	6.62x10-4

Table 2: Aluminum [24, 25, 26, 27]

Aluminum	**Experimental**	**DFT**
a [Å]	4.0495	4.0311
V [Å^3]	66.4055	65.5044
B (GPa)	76	77.1(5)
Young's Modulus (GPa)	70	76
Shear Modulus (GPa)	26	26
Poisson Ratio	0.35	0.35

Table 3: Beryllium [28, 29]

Beryllium	Experimental	DFT
a [Å]	2.2858	2.247272
c [Å]	3.5843	3.523017
V [$Å^3$]	16.2181	15.4084
C11 (GPa)	293.6	310(2)
C12 (GPa)	26.8	25(2)
C13 (GPa)	14.0	9.2(2)
C33 (GPa)	356.7	376(1)
C44 (GPa)	162.2	166.3(7)
B (GPa)	116.8	119.8(6)
Young's Modulus (GPa)	315.2	330
Shear Modulus (GPa)	150.1	157
Poisson Ratio	0.032-0.05	0.044

Table 4: UBe_{13} [9, 14, 30, 31]

UBe13	Experimental	DFT
a [Å]	10.268(2) [14] 10.2545-10.2656 [9] 10.2516-10.2561 (this work, see Table 5)	10.1071
C11 (GPa)	310(9)	284(2)
C12 (GPa)	-1(9)	23.3(2)
C44 (GPa)	161(5)	125(1)
B (GPa)	130 108	120(1)
Young's Modulus (GPa)		76
Shear Modulus (GPa)		26
Poisson Ratio		0.35

Table 5: Neutron diffraction results from Rietveld refinement. Error in last digit in parenthesis

Parameter	Single crystal specimen (ID #1986)	Polycrystalline specimen (ID #3318)	Difference (in sigmas)	Difference (in %)
Lattice parameter a [Å]	10.2561(1)	10.2516(1)	45 σ	-0.044%
Unit cell volume [Å^3]	1078.82(4)	1077.39(4)	35.75	-0.13
Uiso U *8a* [Å^2]	0.0081(2)	0.0088(2)	3.5	8.64
Uiso Be1 *8b* [Å^2]	0.0086(2)	0.0086(2)	0	0
U11 Be2 *96i*	0.0105(1)	0.0100(1)	5	-4.76
U22 Be2 *96i*	0.0116(1)	0.0108(1)	8	-6.90
U33 Be2 *96i*	0.0089(1)	0.0090(1)	1	1.12
U23 Be2 *96i*	-0.0002(1)	0.0000(1)	2	--
y Be2 *96i*	0.11509(2)	0.11494(2)	7.5	-0.13
z Be2 *96i*	0.17617(2)	0.17627(2)	5	0.057
Be1-Be2 [Å]	2.1582(2)	2.1573(2)	4.5	-0.04
Be2-Be2 [Å]	2.2306(3)	2.2309(3)	1	0.01
U-Be2 [Å]	3.0103(1)	3.0095(1)	8	-0.03